Available online at www.sciencedirect.com

ScienceDirect

Procedia Manufacturing 50 (2020) 291–297

Procedia MANUFACTURING

www.elsevier.com/locate/procedia

18th International Conference Metal Forming 2020

Relation between microstructure and mechanical properties on intercritically deformed low carbon steels

U. Mayo[a,b,*], N. Isasti[a,b], J.M. Rodriguez-Ibabe[a,b], P.Uranga[a,b]

[a]*Ceit, Manuel Lardizabal 15, 20018 Donostia / San Sebastián, Spain, Member of Basque Research & Technology Alliance (BRTA)*
[b]*Universidad de Navarra, Tecnun, Manuel Lardizabal 13, 20018 Donostia / San Sebastián, Spain*

* Corresponding author. Tel.: +34 943 212 800; *E-mail address:* umayo@ceit.es

Abstract

Intercritical rolling is often applied in order to improve the mechanical properties of heavy gauge structural steel plates. However, these products have large temperature and deformation gradients both over thickness and width, being the control of the process very complex. Considering this issue, it is important to analyze the microstructural evolution under intercritical conditions and how the different process parameters like deformation temperature, chemical composition etc. influence on the final mechanical properties. For that purpose, plane strain compression tests simulating intercritical rolling conditions were carried out for a CMn and a NbV microalloyed steel. Tensile tests perfomed for various austenite-ferrite contents prior to the last deformation, show that the reduction of deformation temperature increases strength properties. However, ferrite fractions higher than 25% prior to the last deformation, reduce significantly the ductility. These analyses give the necessary background for the definition of stable process windows that optimize the strength-ductility property balance of intercritically rolled products. Similarly, the estimation of the contribution of different strengthening mechanisms such as, solid solution, grain size and dislocation density, allows the prediction of the yield strength of an intercritically deformed microstructure.

Keywords: Intercritical deformation; microalloyed steel; mechanical properties

1. Introduction

Intercritical rolling is widely employed in the production of heavy gauge structural plates in order to fulfill the most demanding mechanical property requirements of several structural applications, especially related to tensile property demands. This rolling process is characterized by the application of the final deformation passes within the austenite - ferrite biphasic region. Even though rolling in the biphasic region has already been examined for plain carbon steels [1], the exact effect of different process parameters on the evolution of intercritically deformed microstructures for microalloyed steels is not fully understood and its relation with the resulting microstructure and mechanical properties is still unclear [2].

Therefore, a deeper understanding of the microstructural evolution under intercritical conditions and the influence of different austenite–ferrite balances at high temperature is required for microalloyed steels in order to define stable processing windows. A stable process window can only be achieved by a more profound understanding of the microstructure development during the intercritical rolling and its relations with the final microstructure and properties. For that purpose, EBSD based characterization procedures developed recently in this field [3, 4] provide a powerful tool to carry out an in depth analysis of an intercritically deformed microstructure.

At room temperature, the microstructure of an intercritically rolled steel is composed of a mixture of deformed and non - deformed ferrite grains, together with a small amount of

10.1016/j.promfg.2020.08.054

a secondary transformation product, usually pearlite. As in a composite material, the final mechanical properties of intercritically deformed products depend on the amount and characteristics of each phase. Due to the complex interaction between deformation, softening mechanisms (recrystallization and recovery) and phase transformation processes in the intercritical temperature range, the estimation of intercritically deformed microstructure properties becomes complex. With the aim of modelling the yield strength, a nonlinear law of mixture [5] is proposed, where the contribution of the different strengthening mechanisms was calculated individually for each ferrite population (Non-deformed and deformed ferrite).

2. Material and methods

In the current work, and in order to simulate intercritical rolling conditions, plane strain compression tests were performed. For that purpose, a servo-hydraulic INSTRON 1344 press was employed. The compression machine has attached an induction furnace to control the heating of the tool and the specimen during the trial. Specimens are 60 mm long, 30 mm wide and 13.5 mm thick. Boron nitride was used as a lubricant, with an estimated friction coefficient of μ=0.15. The specimens used for the microstructural and mechanical characterization were machined from the central area of the plane strain compression sample in order to minimize strain gradients [6].

A low carbon steel (with 0.06% C), as well as a NbV microalloyed steel were selected to carry out the simulation of an intercritical rolling schedule. The chemical compositions of the steels are listed in Table 1.

Table 1. Chemical composition of the studied steels (weight percent).

Steel	C	Mn	V	Ti	Al	Nb	N
CMn	0.063	1.53	0.005	0.002	0.035	0.002	0.003
NbV	0.062	1.52	0.034	0.002	0.038	0.056	0.004

With the aim of analyzing the effect of different process parameters such as, chemical composition and austenite condition, different thermomechanical schedules were designed, as shown in Fig. 1 (Cycle A for CMn and NbV Rex γ samples, whereas Cycle B for NbV Def γ). In order to dissolve all the microalloying elements, both schemes include a solubilization step performed at 1250º C during 10 minutes. Afterwards, a deformation of 0.4 was applied at 1050ºC in both cycles, with the aim of obtaining a recrystallized austenite prior to transformation. However, in some of the NbV steel samples (see Cycle B in Fig. 1b), a second deformation pass was applied below the non-recrystallization temperature (900ºC), in order to accumulate deformation in the austenite prior to transformation. Then, samples were cooled down slowly (1ºC/s) to four different deformation temperatures. For obtaining fully austenitic and ferritic microstructures prior to the last deformation, deformation temperatures of 800 ºC and 650 ºC were defined, named as Tdef0 and Tdef100, respectively (0% and 100% of ferrite prior to the last deformation pass). In the intercritical region, two different deformation temperatures were defined in order to achieve 25 and 75% of ferrite content prior to deformation (Tdef25 and Tdef75, respectively). For CMn steel, deformation temperatures of 705 and 685 ºC were defined, for Tdef25 and Tdef75, respectively. In the NbV Rex γ sample, deformation temperatures of 700 and 685 ºC were defined, whilst, for NbV Def γ, deformation temperatures of 715 and 700 ºC were selected, respectively. Finally, a deformation step of 0.4 was applied in all the deformation temperatures, concluding the cycle with a slow cooling at a rate of 1ºC/s.

The microstructural characterization was carried out by optical microscopy and field-emission gun scanning electron microscopy (FEG-SEM). For that purpose, samples were first mechanically ground with SiC abrasive papers to be later polished with diamond liquids of 6, 3 and 1 µm, subsequently. Finally, the specimens were etched in 2% Nital in order to reveal the microstructure.

EBSD sample preparation was based on the previously mentioned polishing route, using diamond liquid down to 1 µm, followed by a final polishing with a 50 nm colloidal silica suspension during 30 minutes. Orientation imaging microscopy was performed on the Philips XL 30CP SEM microscope, using TSL equipment. A step size of 0.5 µm was defined, with a total scanned area of 350×350 µm^2.

In addition to the microstructural characterization performed on the central part of the plane strain compression specimens, two cylindrical tensile samples (diameter of 4 mm and gauge length of 17 mm) were also machined in each case from the previously tested plane compression samples. The tensile tests were carried out in an INSTRON 5982 machine, with displacement control. The trials were performed in accordance to ASTM E8M standard. In the current study, a deformation rate of 0.9 mm/min was imposed, with a load cell of 20 kN. The strain was measured with a strain-gauge extensometer over a 12.5 mm gauge-length.

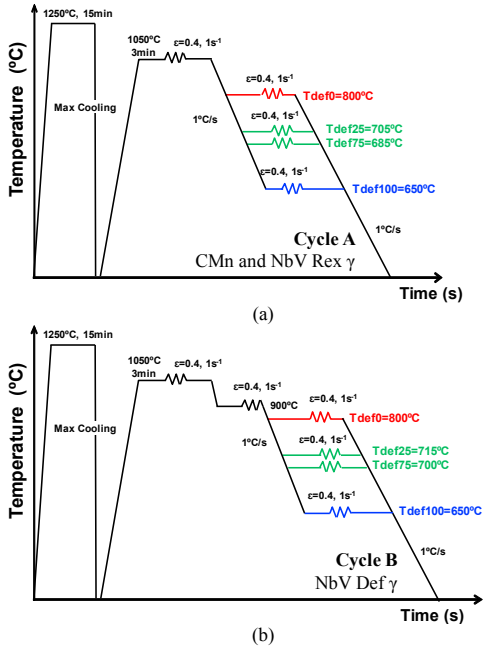

Fig. 1. Thermomechanical cycles applied in plane compression tests: (a) Cycle A for CMn and NbV Rex γ and (b) Cycle B for NbV Def γ steel.

3. Results and discussion

3.1. Characterization of the air cooled samples

Fig. 2 illustrates the optical micrographs corresponding to NbV Rex γ and different deformation temperatures of Tdef0, Tdef25, Tdef75 and Tdef100. For Tdef0, when the last deformation pass is applied in the austenitic region (at 800 ºC), the microstructure is mainly composed by polygonal ferrite grains together with a small fraction of pearlite (see Fig. 2a). If the final deformation pass is applied in the intercritical region, combinations of non-deformed and deformed ferrite grains are clearly noticed in the resulting microstructure, as shown in Fig. 2b and c. The reduction of the deformation temperature leads to the increment of the deformed ferrite content and therefore, the evidence of substructure is more relevant as Tdef decreases. Finally, when the last deformation pass is applied in the ferritic region (at 650 ºC), the microstructure is composed almost entirely of deformed ferrite grains (see Fig. 2d).

In order to study the misorientation inside each grain, boundary maps measured by EBSD were drawn. Several studies reported that low and high angle unit sizes can be directly related to mechanical properties [7, 8]. Low angle misorientation unit sizes are related to tensile properties, as they are considered an effective barrier to dislocation movement. Conversely, crystallographic units surrounded by high angle boundaries are considered effective in opposing crack propagation and may control toughness.

Fig. 3 shows the grain boundary maps corresponding to NbV Rex ɣ sample and entire range of deformation temperatures. Low (misorientation between 4º and 15º) and high angle boundaries (misorientation > 15º) have been overdrawn in red and black lines, respectively. As shown in Fig. 3, depending on the deformation temperature (and consequently ferrite content prior to the last deformation), the resulting microstructure varies considerably. When the sample is deformed at 800 ºC (Tdef0, see Fig. 3a), an equiaxed ferritic microstructure is noticed, related to the formation of a high fraction of NDF grains which are associated with small low angle boundary fractions. As temperature is reduced to Tdef25 and Tdef75 (intercritical region, see Fig. 3b and c), differences in morphology between NDF and DF grains, previously observed in Fig. 2b and c, become evident. The grain boundary maps shown in Fig. 3b and c suggest that the applied intercritical deformation modifies the ferrite morphology, which is reflected in the presence of a marked substructure (DF grains characterized by high density of LAGBs drawn in red). Conversely, the NDF formed during air cooling, which is formed from a pancaked austenite after the intercritical deformation, is characterized by a small fraction of low angle boundaries. If the deformation temperature is reduced to 650 ºC (Tdef100), deformed ferrite content is increased and almost the entire microstructure is composed by elongated ferrite grains with a significant substructure.

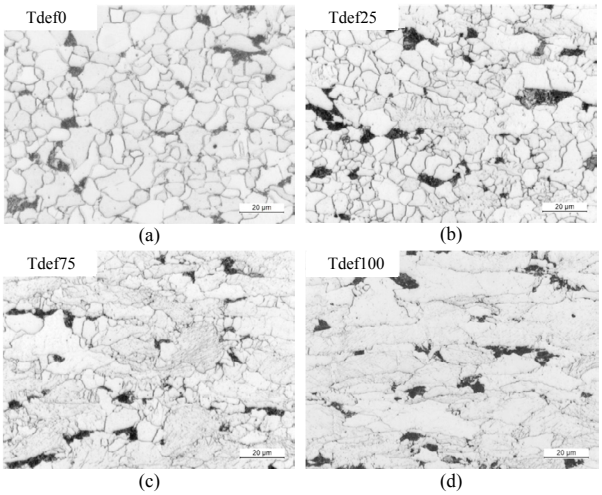

Fig. 2. Optical micrographs corresponding to NbV Rex γ steel, obtained at different deformation temperatures: (a) Tdef0 (austenitic region), (b) Tdef25 (intercritical region, 25% DF), (c) Tdef75 (intercritical region, 75% DF) and (d) Tdef100 (ferritic region).

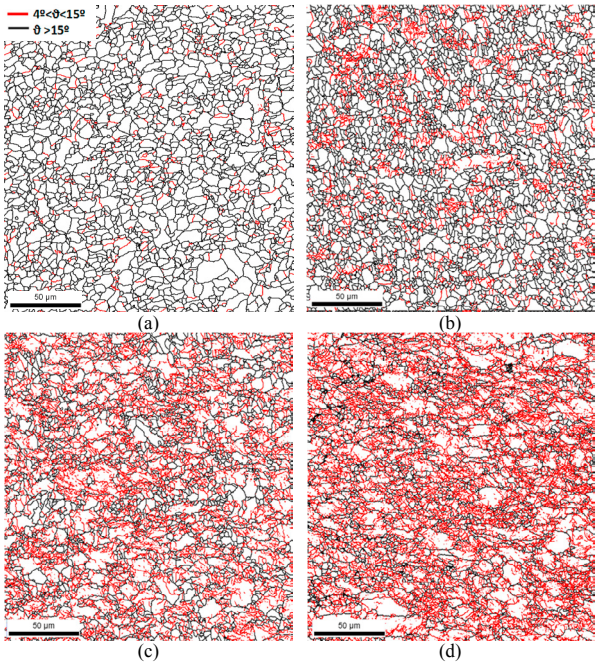

Fig. 3. Grain boundary maps corresponding to NbV Rex γ steel and different deformation temperatures: (a) Tdef0, (b) Tdef25, (c) Tdef75 and (d) Tdef100.

3.2. Discretization methodology

With the aim of characterizing and quantifying the microstructural features of each ferrite type individually, the differentiation between both NDF and DF population is required. For that purpose, a methodology based in grain misorientation was developed using the EBSD technique [3]. The procedure consists of two principal steps: First, in order to distinguish both ferrite populations, pearlite was removed from the analysis. Pearlite was identified using a criterion based on Grain Average IQ parameter, which describes the quality of an electron back scattering diffraction pattern. Being the pearlite a constituent composed of ferrite and cementite, a worst IQ value is expected. In order to remove the corresponding pearlite fraction for each chemistry, austenite condition and deformation temperature, the pearlite fractions were measured by manual point count method from the previously shown optical micrographs (see Fig. 2). Second, the two ferrite types were distinguished based on a grain misorientation based method (GOS). Grain Orientation Spread (GOS) parameter, is the average deviation between the orientation of each point in the grain and the average orientation of the grain. It is supposed that DF grains would achieve higher misorientation values, principally related to the substructure that is generated in such grains.

For each GOS distribution, calculated from the scans performed in the plane compression samples, a threshold GOS value was defined for differentiating between deformed and non-deformed ferrite grains. Similar tolerance angles were determined in all the cases, and a common value of 2º was calculated as the average of all the threshold angles defined in each scan. This minimum GOS value makes it possible to distinguish both NDF and DF grains in the final microstructure for different compositions, ferrite contents and austenite conditions. Grains with GOS values higher than 2º are considered DF grains, whilst grains with GOS values lower than 2º are defined as NDF grains.

In Fig. 5, mean unit size values as a function of the corresponding deformation temperature and different steel grades are plotted for both ferrite types (NDF and DF). Concerning mean unit sizes quantified for the NDF population, the addition of Nb and V promotes the NDF grain size refinement for Tdef0 and Tdef25 conditions. Furthermore, the reduction of the deformation temperature also diminishes the NDF population grain size in all the cases. As the deformation temperature decreases, the microstructure contains higher ferrite content prior to the last deformation and therefore, a lower remaining austenite content, promoting the formation of finer microstructures in the final slow cooling. For example, in the CMn steel mean unit sizes of 9.7 and 2.5 µm are measured, for Tdef0 and Tdef100, respectively.

Regarding the DF family, similar trends are noticed concerning the effect of microalloying elements. Furthermore, for DF family, the influence of ferrite content prior to the final deformation is noticed. Coarser microstructures are achieved as the deformed ferrite fraction increases in all the cases. In NbV Rex γ, mean unit sizes of 6.3, 7.9 and 8.3 µm are quantified, for Tdef25, Tdef75 and Tdef100, respectively.

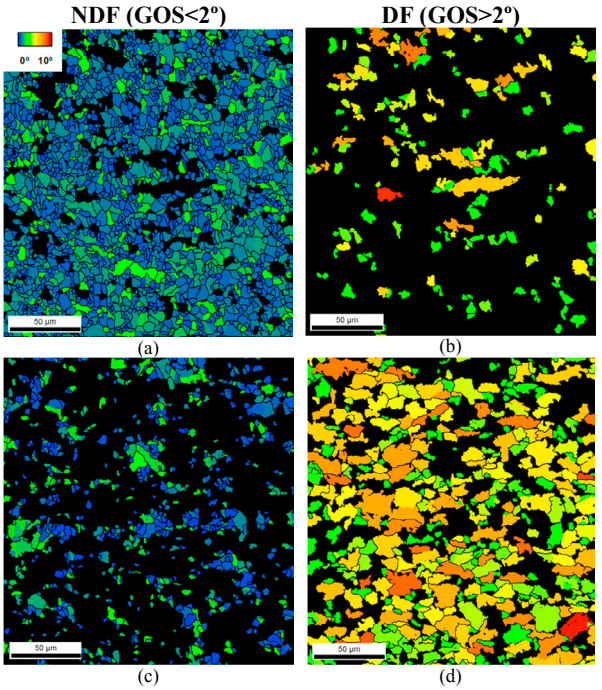

Fig. 4. Grain Orientation Spread maps corresponding to NbV Rex γ (a,b) Tdef25 and (c,d) Tdef75, for both ferrite families: (a,c) NDF (GOS<2º) and (b,d) DF (GOS>2º).

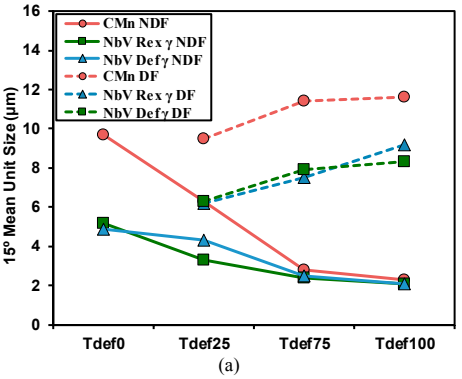

Fig. 5. Mean Unit Sizes considering high angle boundaries corresponding to NDF and DF population, for different chemistries, austenite conditions and entire range of deformation temperatures.

3.3. Interaction between restoration and precipitation

Similar to the precipitation analysis performed in a recently published paper [4], where the interaction between Nb in solution and restoration mechanisms were studied, in the current work a precipitation study was carried out for Tdef75 in both NbV Rex γ and NbV Def γ conditions (deformation temperature of 685 and 700ºC, respectively). As expected, different precipitation patterns are observed depending on the applied austenite conditioning. Comparing the TEM images presented in Fig. 6, a higher fraction of precipitates is detected when the transformation occurs from a recrystallized austenite compared to deformed austenite. Different precipitate populations are observed in both conditions. The deformation

of austenite below the Tnr (non-recrystallization temperature) causes the formation of strain induced precipitates, which are effective delaying recrystallization of austenite and ensuring accumulation of deformation on the austenite prior to transformation (see Fig. 6b). Therefore, the Nb available during or after transformation is reduced, modifying the restoration or recrystallization phenomena occurring during intercritical deformation. When the transformation takes places from a recrystallized austenite, higher precipitation density is noticed and finer particles can be distinguished (see Fig. 6a). These precipitates are supposed to be formed during and/or after intercritical deformation in ferrite. In addition to a higher Nb in solution available, a lower deformation temperature is applied in the NbV Rex γ, ensuring a considerable precipitation refinement. The differences on precipitation and the Nb available to interact with restoration mechanisms, could explain the differences observed in the morphology of the DF population (see Fig. 6c and d). The deformation bands identified in the NbV Rex γ condition (see Fig. 6c) could be related to a delaying of ferrite restoration phenomena caused by Nb in solid solution. Conversely, when the last deformation pass is applied below Tnr (NbV Def γ) the amount of microalloying elements in solution decreases, promoting the activation of restoration phenomena in ferrite during or after intercritical deformation (see Fig. 6d).

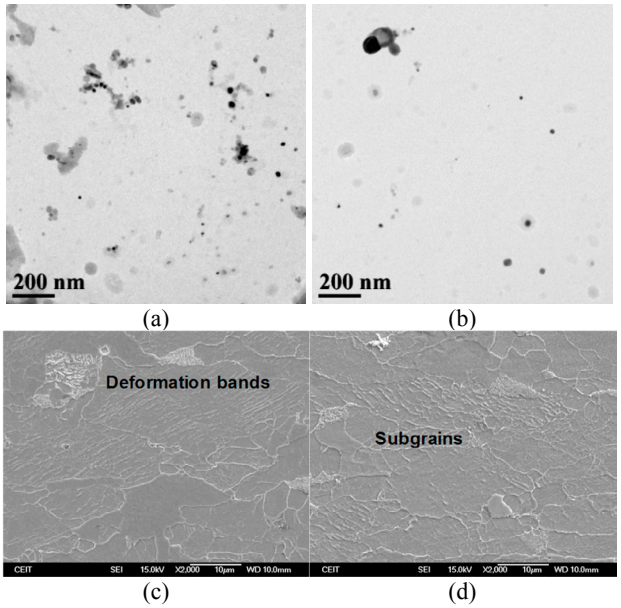

Fig. 6. TEM and FEGSEM micrographs obtained for Tdef75: (a,c) NbV Rex γ and (b,d) NbV Def γ.

3.4. Tensile properties

Fig. 7a shows tensile curves corresponding to NbV Rex ɣ and the entire range of deformation temperatures (Tdef0, Tdef25, Tdef75 and Tdef100). The 2% proof stress and the tensile strength were determined as the average of two tensile tests in each condition. The results suggest that the reduction of the deformation temperature causes the increment of both yield and tensile strength. All the curves show the typical plateau due to a discontinuous yielding behavior, which is associated with the presence of polygonal ferrite in the microstructure.

In Fig. 7b, yield strength values are plotted for both steels, austenite conditions and different deformation temperatures. In terms of the influence of chemistry, the results plotted in Fig. 7b evidence that the addition of microalloying elements promotes the improvement of tensile properties for all the deformation temperatures. Nevertheless, unless for the Tdef0 case, where the difference in grain size between NbV Rex γ and NbV Def γ samples is relevant, no impact of the austenite condition is observed for Tdef25, Tdef75 and Tdef100 cases, as both NbV Rex γ and NbV Def γ samples achieve similar YS values. Regarding the effect of deformation temperature, higher deformation temperatures are related to lower strength properties in all the steels. Attending to Table 2, where the yield and tensile strength values, in conjunction with the elongation are listed for all the conditions, it can be seen that for the NbV Rex γ steel, YS values of 386.4, 412.5, 439.9 and 448 MPa are measured, for Tdef0, Tdef25, Tdef75 and Tdef100, respectively.

Even though tensile property enhancement could be reached by decreasing deformation temperature, the reduction of elongation is significant when the microstructure contains a high ferrite fraction prior to the intercritical deformation (Tdef75 and Tdef100, see Table 2). The loss of elongation becomes considerable when ferrite fractions higher than 25% are presented in the microstructure before last deformation pass. This trend could be observed in all the studied cases. In NbV Rex γ steel, for example, the elongation decreases from 43 to 25.5%, for Tdef0 and Tdef100, respectively.

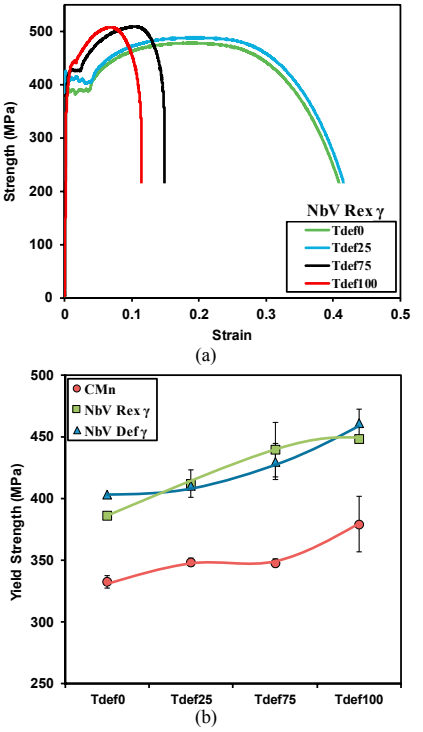

Fig. 7. (a) Influence of deformation temperature on tensile curves for NbV Rex ɣ. (b) Yield Strength as a function of deformation temperature, for both steels and austenite conditions.

Table 2. Measured yield strength, tensile strength and elongation values for both compositions and austenite conditions (CMn, NbV Rex γ and NbV Def γ) and the different deformation temperatures (Tdef0, Tdef25, Tdef75, Tdef100).

	Tdef (ºC)	Yield Strength (MPa)	Tensile Strength (MPa)	Elongation (%)
CMn	Tdef0	332.5±4.9	434.5±3	47.5±1
	Tdef25 705ºC	348.6±3.1	445.1±1.2	46.0±9.7
	Tdef75 685ºC	347.9±3.3	436.5±2.8	31.0±2.9
	Tdef100	379.4±22.2	443.6±2.3	26.0±2
NbV Rex γ	Tdef0	386.4±1.6	476.1±1.5	43.0±2
	Tdef25 700ºC	412.5±11	495.0±16.2	39.5±4.9
	Tdef75 685ºC	439.9±22	507.6±5.1	24.5±3.5
	Tdef100	448.0±1.8	506.0±2.1	25.5±4.8
NbV Def γ	Tdef0	403.6±1.2	481.2±1.9	31.0±1.3
	Tdef25 715ºC	410.3±6.8	485.3±11.5	35.5±3
	Tdef75 700ºC	429.8±14.5	502.9±15.3	29.0±3.9
	Tdef100	460.9±11.6	510.6±4.5	19.0±1.6

3.5. Estimation of the contribution of strengthening mechanisms on yield strength

The strength property of a steel is closely related to the final microstructure, which in turn depends on the chemical composition and the different process variables. Attending to the literature [9, 10, 11], the yield strength of a microalloyed steel is determined by the linear contribution of various strengthening mechanisms, such as, the solid solution, grain size refinement, dislocation density and fine precipitation.

Taking into account that intercritically deformed microstructures are composed by two different ferrite types (NDF and DF), the hardening of the different constituents has to be considered. In order to model the strength behaviour of multiphase steels, nonlinear law of mixtures as presented in Ref [5] can be used, in which the contribution of each phase is related to its fraction. In the current work, based in the aforementioned consideration, a non-linear law of mixtures is proposed, where the contribution of grain size and dislocation density has been calculated separately for each ferrite population (NDF and DF). In this study the contribution concerning precipitation mechanism has been neglected. The precipitation density and the size of the precipitates previously shown in Fig. 6, does not seem to be sufficient to notice a significant impact on the yield strength. Concerning N_{free}%, all the nitrogen is considered to be fully precipitated at room temperature for the NbV steel, whilst for the CMn steel all the N is considered to be in solution. Regarding dislocation density, the contribution of this strengthening mechanism has been evaluated through Kernel Average Misorientation value obtained by EBSD. For NDF, due to the presence of polygonal ferritic grains, dislocation density is considered to be zero.

$$\sigma_y = \sigma_0 + \sigma_{ss} + \left(\sigma_{gsNDF} + \sigma_{\rho NDF}\right)\cdot f_{NDF}^{1/3} + \\ + \left(\sigma_{gsDF} + \sigma_{\rho DF}\right)\cdot\left(1 - f_{NDF}^{1/3}\right) \quad (1)$$

where solid solution (σ_{ss}), grain size (σ_{gs}), dislocation density (σ_ρ) can be calculated with the following equations:

$$\sigma_{ss} = 32.3\,(Mn) + 83.2\,(Si) + 11\,(Mo) + 354\,(N_{free})^{0.5} \quad (2)[11]$$

$$\sigma_{gs} = 17.4 d_\alpha^{-0.5} \quad (3)[12]$$

$$\sigma_\rho = \alpha M \mu b \sqrt{\rho}\,, \quad \rho = \frac{2\theta}{u \cdot b} \quad (4, 5)[13,14]$$

In Fig. 8, the estimated individual strengthening contributions regarding NbV Rex γ sample are presented for different deformation temperatures (Tdef0, Tdef25, Tdef75 and Tdef100). Additionally, the yield strength values measured from the tensile tests are also included. The results suggest that the control of the grain size becomes critical, being the most important strengthening mechanism. In such conditions, it can be seen that the reduction of deformation temperature promotes an increment in the YS value, mainly related to grain refinement. Nevertheless, for Tdef25, Tdef75 and Tdef100, similar grain size contributions are measured. The small differences that are observed in YS strength between these deformation temperatures are related to the dislocation density, which increases as the deformed ferrite fraction increases. The increment of DF fraction involves an increasing of dislocation density, as the value of the kernel increases (see Fig. 3). When the microstructure contains a low deformed ferrite content, the effect of dislocation density is almost negligible. In order to validate the equation, experimental and predicted yield strength values are plotted in Fig. 8b. A good fitting is observed, concluding that a reasonable estimation of yield strength can be achieved considering Eq.1.

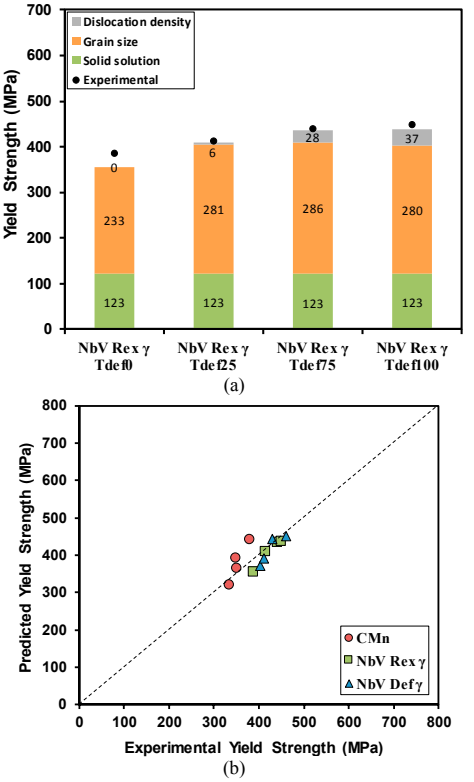

Fig. 8. (a) Contribution of different strengthening mechanisms on the yield strength for NbV Rex γ and entire range of deformation temperatures and (b) Comparison between predicted yield strength considering Eq.1 and experimental yield strength values.

4. Conclusions

Considerably coarser mean grain sizes are quantified for the DF family compared to NDF population. Differences in the average unit sizes are attributed to the initial size and status of the austenite they transform from.

The application of lower deformation temperatures leads to the increment of strength properties, mainly related to a higher fraction of DF grains formed in the final microstructure. Similarly, the addition of Nb and V promotes an improvement in tensile properties, associated to the microstructural refinement and the formation of more bainitic phases with higher dislocation density. However, the loss in ductility for ferrite fractions higher than 25% before the last deformation is very significant, obtaining the best strength-ductility property balance at Tdef25.

A new equation was developed for the prediction of yield strength for intercritically deformed microstructures. The estimation of the contribution of different strengthening mechanisms (grain size, solid solution, and dislocation density) was calculated individually for each ferrite population and the overall response was estimated considering a nonlinear law of mixtures.

Acknowledgements

The financial support of the Spanish Ministry of Economy and Competitiveness (MAT2015-69752) and the European Commission (RFCS-CT-2015-00014) is gratefully acknowledged.

References

[1] Humphreys AO, Liu D, Toroghinejad MR, Essadiqi E, Jonas JJ. Warm rolling behaviour of low carbon steels. Mater Sci Technol 2003;19:709-14.
[2] Simielli EA, Yue S, Jonas JJ. Recrystallization kinetics of microalloyed steels deformed in the intercritical region. Metall Mater Trans A 1992;23:597-608.
[3] Mayo U, Isasti N, Jorge-Badiola D, Rodriguez-Ibabe JM, Uranga P. An EBSD-based methodology for the characterization of intercritically deformed low carbon steel. Mater Charact 2019;147:31-42.
[4] Mayo U, Isasti N, Rodriguez-Ibabe JM, Uranga P. Interaction between Microalloying Additions and Phase Transformation during Intercritical Deformation in Low Carbon Steels. Metals 2019;9:1049-65.
[5] Rodriguez-Ibabe JM. Mellaurgical Aspects of Rolling Process, in The Making, Shaping and Treating of Steels. AIST 2014:113-70.
[6] Uranga P, Gutiérrez I, López B. Determination of recrystallization kinetics from plane strain compression tests. Mater Sci Eng A 2013;578:174-80.
[7] Hanamura T, Yin F, Nagai K. Ductile-brittle transition temperature of ultrafine ferrite/cementite microstructure in a low carbon steel. ISIJ Int 2004;44:610-7.
[8] Isasti N, Jorge-Badiola D, Taheri ML, Uranga P. Phase transformation study in Nb-Mo microalloyed steels using dilatometry and EBSD quantification. Metall Mater Trans A. 2013;44:3552-63.
[9] Gladman T, Dulieu D, McIvor ID. Structure-property relationships in high strength microalloyed steels. In Microalloying 75; 1975. p. 32-55.
[10] Mintz B, Peterson G, Nassar A. Structure-property relationships in ferrite-pearlite steels. Ironmak Steelmak 1994;21:215-22.
[11] Pickering FB, Gladman T. Metallurgical developments in carbon steels. Iron Steel Inst Spec Rep 1963;81:10.
[12] Pickering FB. Physical Metallurgy and Design of Steels. Barking, Essex, United Kingdom: Applied Science Publishers; 1978.
[13] Keh AS, Weissmann S. Deformation subsructure in BCC metals. In Electron Microscopy and the Strength of Crystals, G. Thomas and J. Washburn, Eds. New York, USA: Interscience; 1963. p. 231-300.
[14] Calcagnotto M, Ponge D, Demir E, Raabe D. Orientation gradients and geometrically necessary dislocations in ultrafine grained dual-phase steels studied by 2D and 3D EBSD. Mater Sci Eng A 2010;527:2738–46.